RSC Advances

ROYAL SOCIETY OF CHEMISTRY

www.rsc.org/advances

Silver nanowire electrodes incorporated with polyethoxysiloxane reveal excellent resistance to oxidation and significantly increase conductivity by 1-2 orders of magnitude.

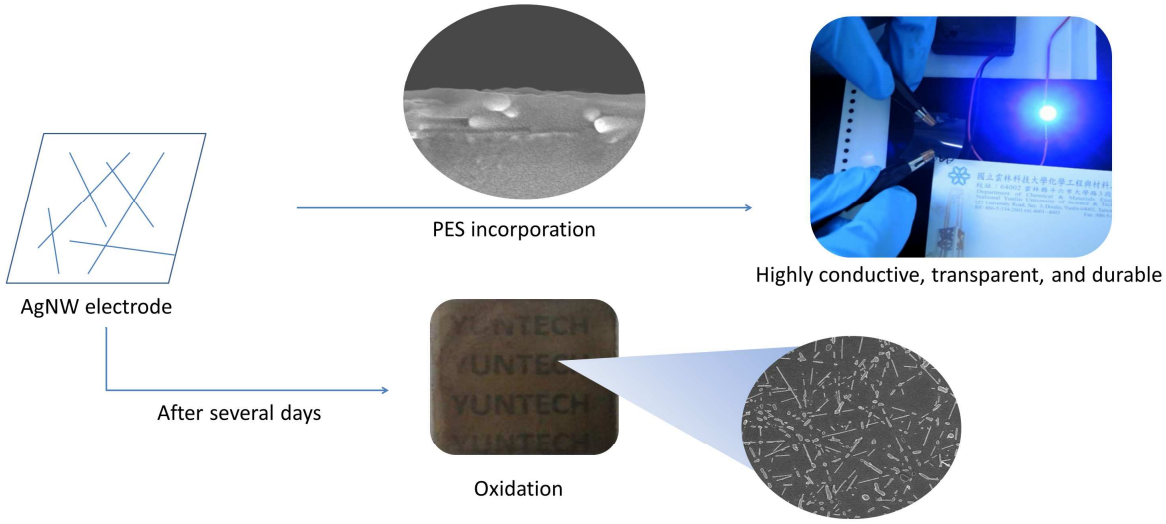

Transparent conductive electrodes of silver nanowires with high resistance to oxidation and thermal shock

Bo-Tau Liu* and Shao-Xian Huang

Department of Chemical and Materials Engineering
National Yunlin University of Science and Technology
Yunlin 64002, Taiwan

*Corresponding author: Department of Chemical and Materials Engineering, National, Yunlin University of Science and Technology, 123 Univ. Rd., Sec. 3, Douliou, Yunlin 64002, Taiwan, ROC. Tel.: 886-5-534-2601. Fax: 886-5-531-2071.
E-mail address: liubo@yuntech.edu.tw (B.-T. Liu).

ABSTRACT

Oxidation was a man issue for the silver-nanowire electrodes when the bulk silver reduces to nano-scale size, restricting it to practical application due to the significant rise of sheet resistance. We reported a simple method by virtue of incorporating polyethoxysiloxane (PES) into silver-nanowire layer to enhance the resistance to oxidation and thermal shock. As a result of the PES incorporation, the temperatures for oxidation to occur were raised from 250 and 300℃ to 300 and 500℃ under air and N_2 atmospheres, respectively. Moreover, after the PES incorporation the silver nanowires became tighter contact in cross connection due to the sol-gel shrinkage, resulting in a near 2-fold enhancement in the conductivity and superior bend performance compared to the pristine AgNWs electrodes. We used the silver-nanowire electrodes incorporated with PES to prepare the G/F/F-stack dual-touch sensor, revealing a rapid response and stable performances more than 3 months.

Key words: Silver nanowire; Polyethoxysiloxane; Transparent electrodes; Sheet resistance

1. **Introduction**

Transparent conductive electrodes are key components of optoelectronic products, such as touch panels, liquid crystal displays, solar cells, and organic light emitting diodes. The most commonly used material in the manufacture of transparent conductive electrodes is indium tin oxide (ITO), as a result of its low electrical resistance and high transparency. As the optoelectronic products become popular and cheap, low-cost or new-function materials for transparent conductive electrodes have received increasing attentions and been seeking over the last two decades. Several new materials, including carbon nanotubes,[1, 2] graphene nanosheets,[3] silver-particle grid [4] and silver nanowires (AgNWs),[5, 6] have been investigated widely as potential replacements for ITO in transparent conductive electrodes to solve the major problems: inflexibility and the limited supply of indium.[7, 8] Moreover, ITO coated on the plastic substrates possesses poor conductivity due to incapable of high-temperature annealing, restricting the development of ITO plastic films. Although all of these candidates possess low-cost and flexible performances, silver materials show the best ratio of DC conductivity to optical conductivity ($\sigma_{DC} / \sigma_{OP}$),[9] which is a key figure of merit for transparent conductive electrodes. Very recently, transparent conductive electrodes made from AgNWs and metal mesh have been applied practically in touch panels by touch-sensor manufacturer, such as TPK Film,

O Film, and Young Fast Optoelectronics.

A number of methods have been shown to successfully fabricate AgNWs, for example, template,[10, 11] hydrothermal,[12, 13] low-temperature growth,[14] thermal-induced formation,[15] microwave assistance[16, 17] and photo-reduction,[18] but the salt-mediated polyol method extended by Xia's group[19-23] is the most impressive and popular because of its simplicity and effectiveness. In the method, the aspect ratio of AgNWs depends strongly on kinds of inorganic salts,[24, 25] ratio of salt to silver nitrate,[26] molecular weight of PVP (polyvinylpyrrolidone),[27] ratio of PVP to silver nitrate,[25] reaction temperature,[26, 28] reaction time,[29] atmosphere,[30, 31] and reagent-addition procedure.[23, 28, 32] Based on these parameters, many efforts have been exerted to control length and diameter of AgNWs to enhance performance on the application of transparent conductive electrodes.[29, 33] However, some critical issues such as low adhesion on substrates and high junction resistance between wires prohibit AgNWs from practice application. A simple method to improve the AgNW adhesion is to cover AgNWs with a resin[6, 34] or stick/bury AgNWs on the surface of a resin layer.[9, 35] As to the junction issue, the post-thermal treatment at ca. 200℃ used to improve the conductivity of AgNW electrodes. Lee et al.[36] supposed that the reduction in junction resistance was attributed to the flowing and partial decomposition of PVP which allowed AgNWs to contact tightly and fuse together; too long thermal-treatment time

or too high thermal-treatment temperature would result in the fact that AgNWs become disconnected droplets, leading to an increase in sheet resistance. Recently, some studies showed that the network-junction resistance could be reduced through sol–gel shrinkage to make AgNWs tighter contact[37] or galvanic displacement of Au to connect the wires.[38] These methods significantly improve the electrical conductivity of transparent conductive electrodes of AgNWs, providing performance comparable to that of commercial ITO films. However, it remains a challenge to develop a facile approach to simultaneously solve the issues of adhesion and junction resistance.

In this study, we incorporated polyethoxysiloxane (PES) into AgNW network and showed significant improvement on both mechanical properties and electrical conductivity. Moreover, resistance to oxidation at elevated temperature increases remarkably, extending applicability in practical products. Effects of PES incorporation on surface-chemical information, mechanical properties, and optical performance of AgNWs were further investigated and analyzed.

2. Experimental

2.1 Materials

Silver nitrate ($AgNO_3$), PVP (MW:40000), and ethylene glycol (EG) were purchased from Sigma–Aldrich. PES (Shin-Etsu), tetrabutyl titanate (TBT, Fluka), sodium

chloride (Katayama Chem., 99.5%) and 2,4-pentanedione (Alfa Aesar) were used as received. Reagent-grade solvents and deionized water (DI water, >18 MΩ·cm) were used throughout the experiments.

2.2 Preparation of AgNWs

AgNWs were synthesized using a two-step polyol reduction method as reported in the previous study.[39] Briefly, 36 mL of 0.3 M PVP and 80 μL of 0.2 M NaCl EG solution were mixed in a reaction vessel and heated at 160 °C. 20 μL of 1 M $AgNO_3$ EG solution was then added into the mixture. After 5 min, a further charge of 1 M $AgNO_3$ (4 mL) was added slowly using a peristaltic pump; when the color of the solution turned to a misty auburn, the residual $AgNO_3$ solution was added into the vessel immediately. After the color of the solution becomes silver-whitish, the as-prepared AgNWs were washed three times with ethanol through centrifugation. The AgNWs had lengths of 10-15 μm and diameters of 60-110 nm.

2.3 Preparation of AgNW layer and thermal treatment

Glass or polyethylene terephthalate (PET) substrates were washed with ethanol and cleaned using an O_2 plasma cleaner (PDC-23G, Harrick Plasma). AgNW solution (2.3 mg/mL) was spin-coated on a treated substrate and then dried at room temperature. The AgNW-coated substrates were placed under a N_2 or an air atmosphere at various temperatures (200, 250, 300, 400, and 500℃) for 20 min.

2.4 PES incorporation

3 g of 0.1 M hydrochloric acid was added into 30 g of PES ethanol solution with various PES contents (0.16, 0.24, 0.38, 1.6, 3.2, 4.8, 6.24, 8, 11.2 wt.%). The mixing solution was heated at 70 °C for 3 h and then cooled to room temperature. The AgNW-coated substrates were dipped in the mixing solution, and subsequently raised immediately from the dipping bath. Upward and downward dipping rates in all experiments were 110 mm/min. The coated samples were placed in an oven at 70℃ for 10 min and then at 100℃ for 3 h to post-cure the PES.

In order to compare effect of the incorporation, the incorporation was also prepared by TiO_2 as suggested elsewhere.[37] TBT and 2,4-pentanedione were mixed in ethanol solution by a weight ratio of 8:1. The total mixture solution is 30 g with various TiO_2 contents (0.16, 0.24, 0.38, 1.6, 3.2, 4.8, 6.24, 8, 11.2 wt.%). The solution was added by a drop of 61% nitric acid and then heated at 70 °C for 3 h. The coating procedure is the same as did for PES incorporation.

2.5 Characterization

The morphologies of the AgNWs, and the PES incorporation were examined using an optical microscope (M835, M&T Optics) and a field-emission scanning electron microscope (JSM-7401F, JEOL). The elemental analysis and binding energy of the surface of the AgNWs were determined by X-ray photoelectron spectroscopy (XPS)

(PHI 5000 VersaProbe, ULVAC-PHI) at a take-off angle of 90^0. The sheet resistances of the transparent conductive electrodes were determined using a four-pin probe meter (Loresta-GP, Mitsubishi Chemical) with an MCP-T610 probe. The transmittance of each sample was measured at four points using an UV–Vis spectrophotometer (Lambda 850, PerkinElmer). Anti-scratch properties of the AgNW electrodes were determined by a motorized abrasion tester (Model 339, Fu-Chien Enterprise Co) with a cotton mat for 10 rounds in a 400 g load. For a bend test, a thin-film sample of 1 cm x 5 cm was made on the PET substrate. It was regarded as a cycle in the bend test that a short edge of the sample was bent to touch the other short edge and then relaxed the sample to be flat.

3. Results and discussion

The pristine AgNW electrodes show a trade-off characteristic that sheet resistance increases with transmittance. As shown in Fig. 1, the performance can be improved by thermal treatment, which may lead to the flowing or partial decomposition of PVP and therefore reduces the junction resistance among AgNWs. Considering the need for gathering basic information on AgNW electrodes for practical applications, performing a systematic analysis is highly desirable. To this end, the AgNW electrodes were treated under N_2 and air atmospheres at various temperatures. As

shown in Fig. 2, the sheet resistance of AgNW electrodes can be reduced by thermal treatment with the temperature below 250℃ (air) and 400℃ (N_2).With increasing temperature, the sheet resistance showed a significant reduce in sheet resistance, reaching a minimum value at 250 and 300℃ under air and N_2 atmospheres, respectively, but then increasing upon increasing temperature furthermore. No matter what kind of atmosphere is used, the sheet resistance of the AgNW electrodes increases remarkably at elevated temperature. However, the increase in sheet resistance is more moderate under N_2 atmosphere than air one. Fig. 3 displays the SEM images of the AgNW electrodes under air and N_2 thermal treatments at various temperatures. Under air atmosphere, the AgNWs start to be broken at 250℃ and are broken down into nanorods and further granulated nanoparticles with the rise of temperature, whereas the AgNWs are still maintained the integrity below 400℃ under N_2 atmosphere. The SEM observation is in good agreement with the results for sheet resistance. Therefore, the rise of sheet resistance induced by thermal treatment may result from the breakdown of AgNWs.

Although the melting point of silver declines with lowering its size, why are there different results for air and N_2 atmospheres? To realize the cause, the chemical compositions on the surface of AgNWs under different conditions of thermal treatment were analyzed (Table 1). Compared to other conditions, thermal treatment

in air results in the results that the oxygen content on the surface of AgNWs increases remarkably and the binding energy of Ag($3d_{5/2}$) is shifted from 368.2 to 367.2 eV (Fig. 4), where the negative binding-energy shift indicates that the metallic state Ag^0 is oxidized to Ag^{2+} due to the non-electronegativity effect.[40-42] We speculate the reason why the AgNWs are broken more easily under air than N_2 is mainly because of the oxidation of AgNWs. In fact, while the electrodes is exposed to air atmosphere at room temperature, even without thermal treatment, the sheet resistance of pristine AgNW electrodes increases gradually (Fig. 5) and their color becomes dark brown (Fig.6).

In order to prevent the oxidation and improve the poor mechanical property, we incorporated the PES into the AgNW layer (PES-AgNW). We found that the PES incorporation significantly improve the resistance to oxidation/thermal attack on the AgNW electrodes, thermally stabilizing until 300℃ and 500℃ for air and N_2, respectively (Fig. 7). Table 2 shows the electrical property and the anti-scratch of the AgNW electrodes incorporated with various PES content. With increasing the PES content (over 3.2 wt.%), the PES-AgNW electrodes show superior anti-scratch (Table 2) and resistance to oxidation (Fig. 6) compared to the pristine AgNW electrodes. Most notably, the PES incorporation also reduces sheet resistance by 1-2 orders of magnitude, being similar to the effect of thermal treatment. The significant reduction

in sheet resistance does not occur at the resin incorporation.[6, 9] As can been seen in the cross-sectional SEM images of the AgNWs electrodes (Fig.8), the AgNWs become tighter contact in cross connection after the PES incorporation, which may be caused by the sol-gel shrinkage. The closer contact may lead to lowering the resistance at the junctions of the AgNWs to enhance the conductivity of the AgNW electrodes, which is not observed in the carbon-nanotube electrodes.[8] It has been reported that TiO_2 also induce the sol-gel shrinkage to improve the connection of AgNWs (TiO_2-AgNW).[37] Compared PES with TiO_2, Table 2 shows that both incorporations have the similar effect on the conductive and mechanical enhancement. However, too high TiO_2 content results in the rise of electric resistance and the decline of anti-scratch. Fig. 9 shows the surface morphologies of the PES-AgNW and the TiO_2-AgNW. In low solid content, PES forms a uniform layer, whereas TiO_2 reveals as granulated particles. While the solid content is high, obvious cracks appear in the TiO_2 layer and the cracks even break AgNWs (Fig. 9g-h). It might be explained why the electrical and mechanical properties become poor in high TiO_2-content incorporation.

In the previous study for CNT electrodes,[8] a near 100-nm incorporation layer which thickness conforms to the requirement of anti-reflection structure will reduce reflectance and consequently increase transmittance. According to Fresnel theory, to achieve optimal transmittance with respect to the incident wavelength λ, the

incorporation layer of thickness d (if its extinction coefficient is negligible) should satisfy the criterions: $d = \lambda/4n_c$ and $n_c = \sqrt{n_0 n_s}$, where n_c, n_0, and n_s are the refractive indices of the over coat, air, and substrate, respectively.[43, 44] In the present cases, the value of substrate (glass) is near 1.5, and thus the optimal refractive index of the incorporation layer is about 1.22; too low or too high refractive index will lead to high reflectance and low transmittance. The corresponding optimal coating thickness is near 113 nm if the incident wavelength is 550 nm. For most optical materials, their refractive indices are greater than 1.22, and thereby low-refractive-index-material hybrid or homogenous porous formation ($n_0 = 1$) have been widely utilized to reduce the refractive index. On the contrary, the refractive index of silver is a function of incident wavelength and is very low in the visible-light region (0.07-0.09; much lower than that of air).[45] The incorporated material having higher refractive index is easier to make the incorporation layer to reach optimal value. The refractive index of TiO_2 is much higher than that of PES. However, Fig. 10 shows that the electrodes incorporated with PES reveal superior transmittance compared to those incorporated with TiO_2. It may be explained with the fact that that numerous air voids among TiO_2 particles (Figs. 9f-h) deteriorate the light transmission due to refractive-index reduction. Besides, a great difference between the refractive index of TiO_2 and that of AgNWs will induce more significant light scattering compared to the

PES-AgNWs. Observing Fig. 8b, the diameter of AgNWs is comparable to the layer thickness or the optimal thickness. Therefore, the effective homogenous model is inappropriate to the present cases and the light scattering is inevitable. It may explain that, regardless of what the composition is, both PES and TiO_2 incorporations on AgNW electrodes decrease the transmittance (Fig. 10).

Based on the aforementioned results, the PES incorporation reveals superior characteristics on electrical, optical, and mechanical aspects compared to the TiO_2 incorporations. A bend test was also conducted to investigate the effect of PES incorporation on the flexible application. Fig. 11 shows that the sheet resistance of the PES-AgNW electrode remained almost unchanged at the end of 500 cycles, whereas that of the pristine AgNW electrode (without PES incorporation) increased by near 3 times. The result indicates that the PES solidifies the AgNWs and thus increases the reliability of electrodes. We have used the PES-AgNW electrodes (transmittance = 89%; sheet resistance = 100 Ω/sq) to prepare the glass/film/film-stack (G/F/F-stack) dual-touch sensor, as shown in Fig. 12. Two PES-AgNW PET films were sacked under a cover glass for capacitive sensor. The circuit pattern of the PES-AgNW electrodes was carried out by laser etching. The as prepared touch sensor was evaluated using the eGalaxTuner software (see supplementary information). The touch sensor reveals a rapid response and stable performances more than 3 months.

4. Conclusion

We have fabricated highly conductive PES-AgNW electrodes by virtue of incorporating PES into AgNWs. The PES incorporation results in a near 2-fold enhancement in the conductivity compared to the pristine AgNWs electrodes. The improvement may be attributed to the closer touch due to the sol-gel shrinkage. Compared with TiO_2-AgNW electrodes, the PES-AgNW ones show superior optical and mechanical properties as a result of formation of a compact layer. The PES-AgNW electrodes also reveal well resistance to oxidation (300℃ in air; 500℃ in N_2) and excellent bend-test performance (500 cycles), and have been qualified successfully by the practical application in the touch sensor..

Acknowledgments

This study was supported financially by the Ministry of Science and Technology of the Republic of China.

References

1. Z. Wu, *Science*, 2004, **305**, 1273-1276.
2. B. T. Liu, C. H. Hsu and W. H. Wang, *J. Taiwan Inst. Chem. Eng.*, 2012, **43**, 147-152.
3. L. G. De Arco, Y. Zhang, C. W. Schlenker, K. Ryu, M. E. Thompson and C. W. Zhou, *ACS Nano*, 2010, **4**, 2865-2873.
4. B. Y. Ahn, D. J. Lorang and J. A. Lewis, *Nanoscale*, 2011, **3**, 2700-2702.
5. A. R. Madaria, A. Kumar, F. N. Ishikawa and C. W. Zhou, *Nano Research*, 2010, **3**, 564-573.
6. C. H. Liu and X. Yu, *Nanascale Res. Lett.*, 2011, **6**, 75.
7. A. Rahy, P. Bajaj, I. H. Musselman, S. H. Hong, Y.-P. Sun and D. J. Yang, *Appl. Surf. Sci.*, 2009, **255**, 7084-7089.
8. B. T. Liu and C. H. Hsu, *J. Colloid Interface Sci.*, 2011, **359**, 423-427.
9. X. Y. Zeng, Q. K. Zhang, R. M. Yu and C. Z. Lu, *Adv. Mater.*, 2010, **22**, 4484-4488.
10. T. A. Crowley, K. J. Ziegler, D. M. Lyons, D. Erts, H. Olin, M. A. Morris and J. D. Holmes, *Chem. Mater.*, 2003, **15**, 3518-3522.
11. E. Braun, Y. Eichen, U. Sivan and G. Ben-Yoseph, *Nature*, 1998, **391**, 775-778.

12. T. Tetsumoto, Y. Gotoh and T. Ishiwatari, *J. Colloid Interface Sci.*, 2011, **362**, 267-273.

13. J. Xu, J. Hu, C. J. Peng, H. L. Liu and Y. Hu, *J. Colloid Interface Sci.*, 2006, **298**, 689-693.

14. S. H. Kim, B. S. Choi, K. Kang, Y. S. Choi and S. I. Yang, *J. Alloys Compd.*, 2007, **433**, 261-264.

15. T. K. Chen, W. T. Chen, M. C. Yang and M. S. Wong, *J. Vac. Sci. Technol., B*, 2005, **23**, 2261-2265.

16. M. Tsuji, Y. Nishizawa, K. Matsumoto, N. Miyamae, T. Tsuji and X. Zhang, *Colloids Surf. A*, 2007, **293**, 185-194.

17. L. F. Gou, M. Chipara and J. M. Zaleski, *Chem. Mater.*, 2007, **19**, 1755-1760.

18. Z. Xie, Z. Y. Wang, Y. X. Ke, Z. G. Zha and C. Jiang, *Chem. Lett.*, 2003, **32**, 686-687.

19. Y. G. Sun, B. Gates, B. Mayers and Y. N. Xia, *Nano Lett.*, 2002, **2**, 165-168.

20. Y. G. Sun and Y. N. Xia, *Adv. Mater.*, 2002, **14**, 833-837.

21. K. E. Korte, S. E. Skrabalak and Y. N. Xia, *J. Mater. Chem.*, 2008, **18**, 437-441.

22. Y. G. Sun, B. Mayers, T. Herricks and Y. N. Xia, *Nano Lett.*, 2003, **3**, 955-960.

23. Y. G. Sun, Y. D. Yin, B. T. Mayers, T. Herricks and Y. N. Xia, *Chem. Mater.*,

2002, **14**, 4736-4745.

24. C. Chen, L. Wang, G. H. Jiang, J. F. Zhou, X. Chen, H. J. Yu and Q. Yang, *Nanotechnology*, 2006, **17**, 3933-3938.

25. D. P. Chen, X. L. Qiao, X. L. Qiu, J. G. Chen and R. Z. Jiang, *J. Mater. Sci. - Mater. Electron.*, 2011, **22**, 6-13.

26. X. L. Tang, M. Tsuji, M. Nishio and P. Jiang, *Bull. Chem. Soc. Jpn.*, 2009, **82**, 1304-1312.

27. Y. C. Lu and K. S. Chou, *Nanotechnology*, 2010, **21**, 215707.

28. S. Coskun, B. Aksoy and H. E. Unalan, *Cryst. Growth Des.*, 2011, **11**, 4963-4969.

29. S. M. Bergin, Y. H. Chen, A. R. Rathmell, P. Charbonneau, Z. Y. Li and B. J. Wiley, *Nanoscale*, 2012, **4**, 1996-2004.

30. X. L. Tang, M. Tsuji, P. Jiang, M. Nishio, S. M. Jang and S. H. Yoon, *Colloids Surf. A*, 2009, **338**, 33-39.

31. B. Wiley, T. Herricks, Y. G. Sun and Y. N. Xia, *Nano Lett.*, 2004, **4**, 1733-1739.

32. M. J. Hu, J. F. Gao, Y. C. Dong, S. L. Yang and R. K. Y. Li, *RSC Adv.*, 2012, **2**, 2055-2060.

33. S. Sorel, P. E. Lyons, S. De, J. C. Dickerson and J. N. Coleman,

Nanotechnology, 2012, **23**, 185201.

34. M. J. Hu, J. F. Gao, Y. C. Dong, K. Li, G. C. Shan, S. L. Yang and R. K. Y. Li, *Langmuir*, 2012, **28**, 7101-7106.

35. W. Gaynor, G. F. Burkhard, M. D. McGehee and P. Peumans, *Adv. Mater.*, 2011, **23**, 2905-2910.

36. J. Y. Lee, S. T. Connor, Y. Cui and P. Peumans, *Nano Lett.*, 2008, **8**, 689-692.

37. R. Zhu, C. H. Chung, K. C. Cha, W. B. Yang, Y. B. Zheng, H. P. Zhou, T. B. Song, C. C. Chen, P. S. Weiss, G. Li and Y. Yang, *ACS Nano*, 2011, **5**, 9877-9882.

38. L. B. Hu, H. S. Kim, J. Y. Lee, P. Peumans and Y. Cui, *ACS Nano*, 2010, **4**, 2955-2963.

39. B.-T. Liu and H.-L. Kuo, *Carbon*, 2013, **63**, 390-396.

40. J. F. Weaver and G. B. Hoflund, *J. Phys. Chem.*, 1994, **98**, 8519-8524.

41. S. W. Gaarenstroom and N. Winograd, *J. Chem. Phys.*, 1977, **67**, 3500-3506.

42. P. Sangpour, A. Babapour, O. Akhavan and A. Z. Moshfegh, *Surf. Interface Anal.*, 2009, **41**, 157-163.

43. H. A. Macleod, *Thin-film optical filters*, Institute of Physics Pub., Philadelphia, 2001.

44. B.-T. Liu and W.-D. Yeh, *Colloids Surf. A*, 2010, **356**, 145-149.

45. G. Hass and L. Hadley, *Optical constants of metals*, in *American Institute of Physics Handbook*, D.E. Gray, Ed., McGraw-Hill, New York, 1972.

List of figures

Fig. 8. Cross-sectional SEM images of the AgNW electrodes (a) without and (b) with PES incorporation.

Fig. 9. SEM images of the AgNW electrodes dipped in various (a-d) PES and (e-h) TiO_2 concentrations: (a, e) 0.16 wt.%, (b, f) 1.6 wt.%, (c, g) 8 wt.%, and (d, h) 11.2 wt.%. The inset image in (g) and the arrows in (f) indicate the broken AgNWs.

Fig. 10. Transmission spectra of the (a) PES-AgNW and (b) TiO_2-AgNW electrodes made from various dipping concentration.

Fig. 11. Variation of the relative sheet resistance of the pristine AgNW electrode and the 3.2 wt.% PES-AgNW electrode as a function of bending cycles. R_0 is the initial sheet resistance, and R is the sheet resistance after the bending test.

Fig. 12. Photograph of the touch sensor made from the PES-AgNW electrodes.

Table 1. XPS analysis of the surface of the AgNWs thermally treated at 300℃ under different atmospheres.

Samples	Compositions, at.%		$Ag(3d_{5/2})$, eV
	O	Ag	
Pristine AgNWs	10.2	89.8	368.2
AgNWs under air atmosphere	28.1	71.9	367.2
AgNWs under N_2 atmosphere	15.7	84.3	368.2

Table 2. Variation of the relative sheet resistance of the AgNW electrodes after various incorporations and anti-scratch test.

Sample No.		1	2	3	4	5	6	7	8	9
Concentration of coating solution (wt.%)		0.16	0.24	0.38	1.6	3.2	4.8	6.24	8	11.2
PES incorporation	R/R_0	0.058	0.181	0.075	0.015	0.123	0.085	0.063	0.089	0.039
	R_A/R_0	-[a]	-[a]	-[a]	0.543	0.142	0.083	0.066	0.097	0.041
TiO_2 incorporation	R/R_0	0.090	0.152	0.041	0.138	0.219	0.206	0.051	0.056	$1.948*10^4$
	R_A/R_0	-[a]	-[a]	-[a]	1.499	0.220	0.189	0.047	0.063	$1.139*10^9$

R_0: the surface resistance of the pristine AgNW sample.

R: the surface resistance of the AgNW sample incorporated with PES or TiO_2 before the anti-scratch test.

R_A: the surface resistance of the AgNW sample incorporated with PES or TiO_2 after the anti-scratch test.

[a] the AgNW layer was wiped off.

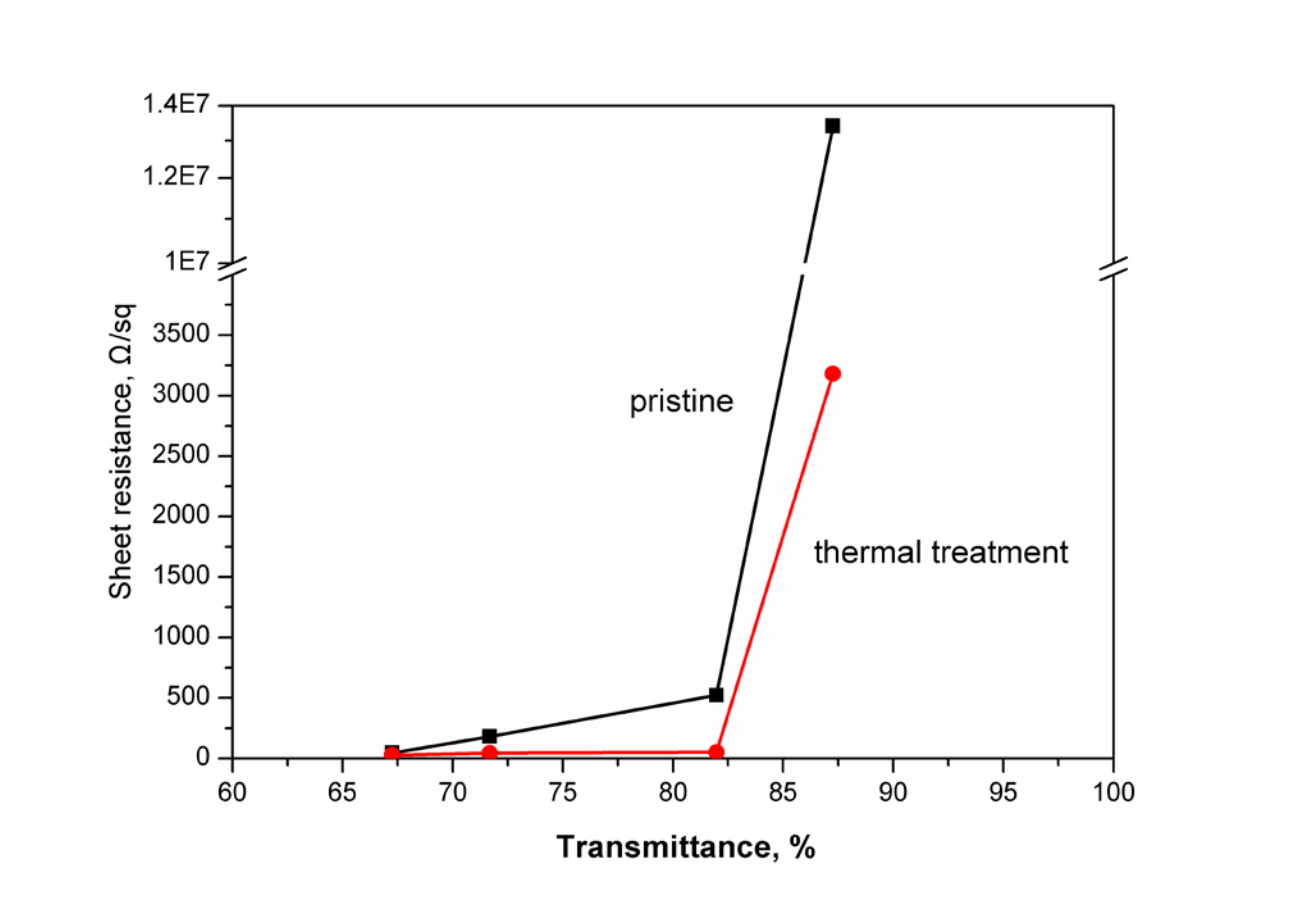

Fig. 1. Variation of the sheet resistance of the AgNW electrodes as a function of transmittance.

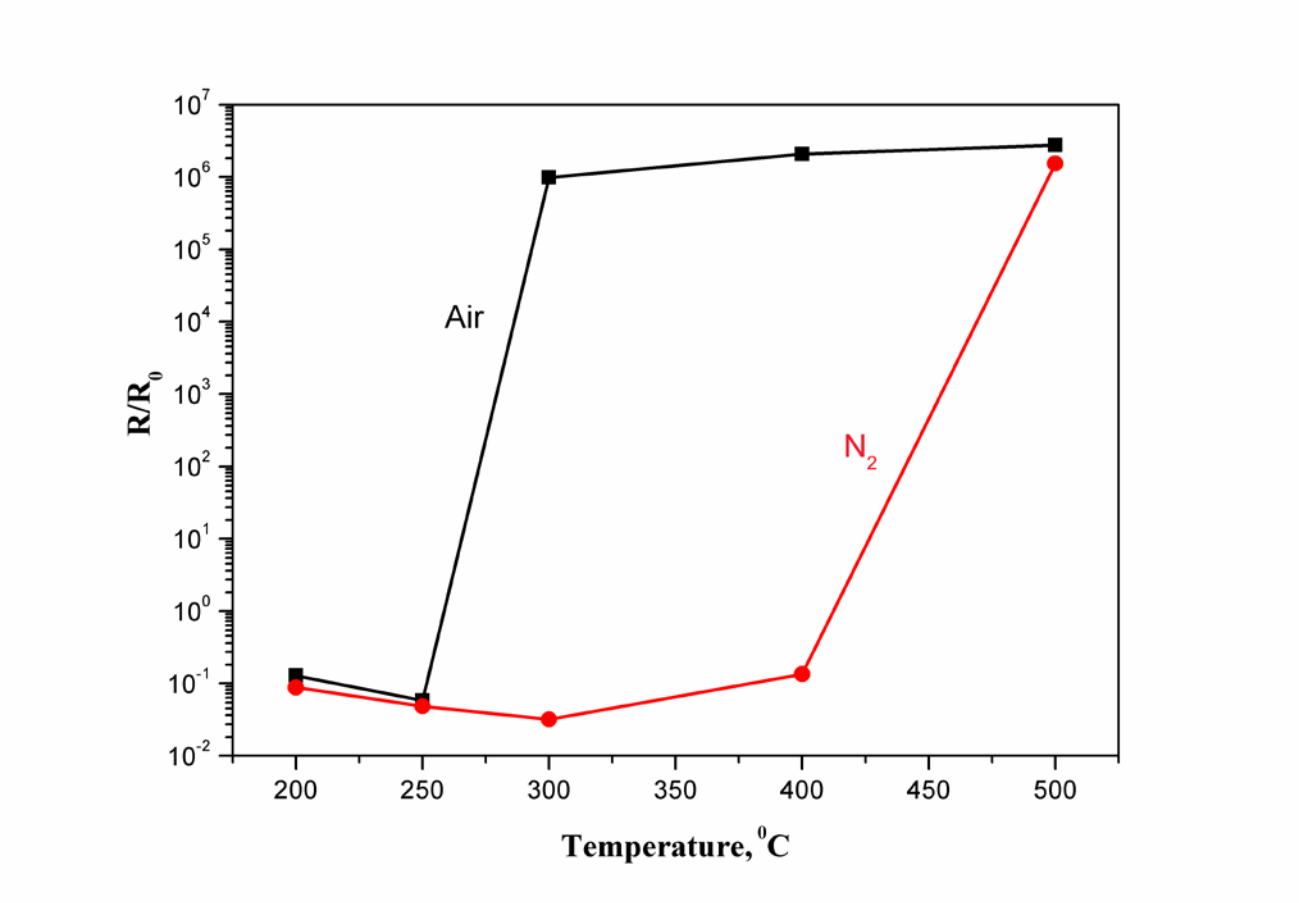

Fig. 2. Variation of the relative sheet resistance of the AgNW electrodes as a function of the thermal-treatment temperature under various atmospheres. R_0 is the initial sheet resistance, and R is the sheet resistance after thermal treatment.

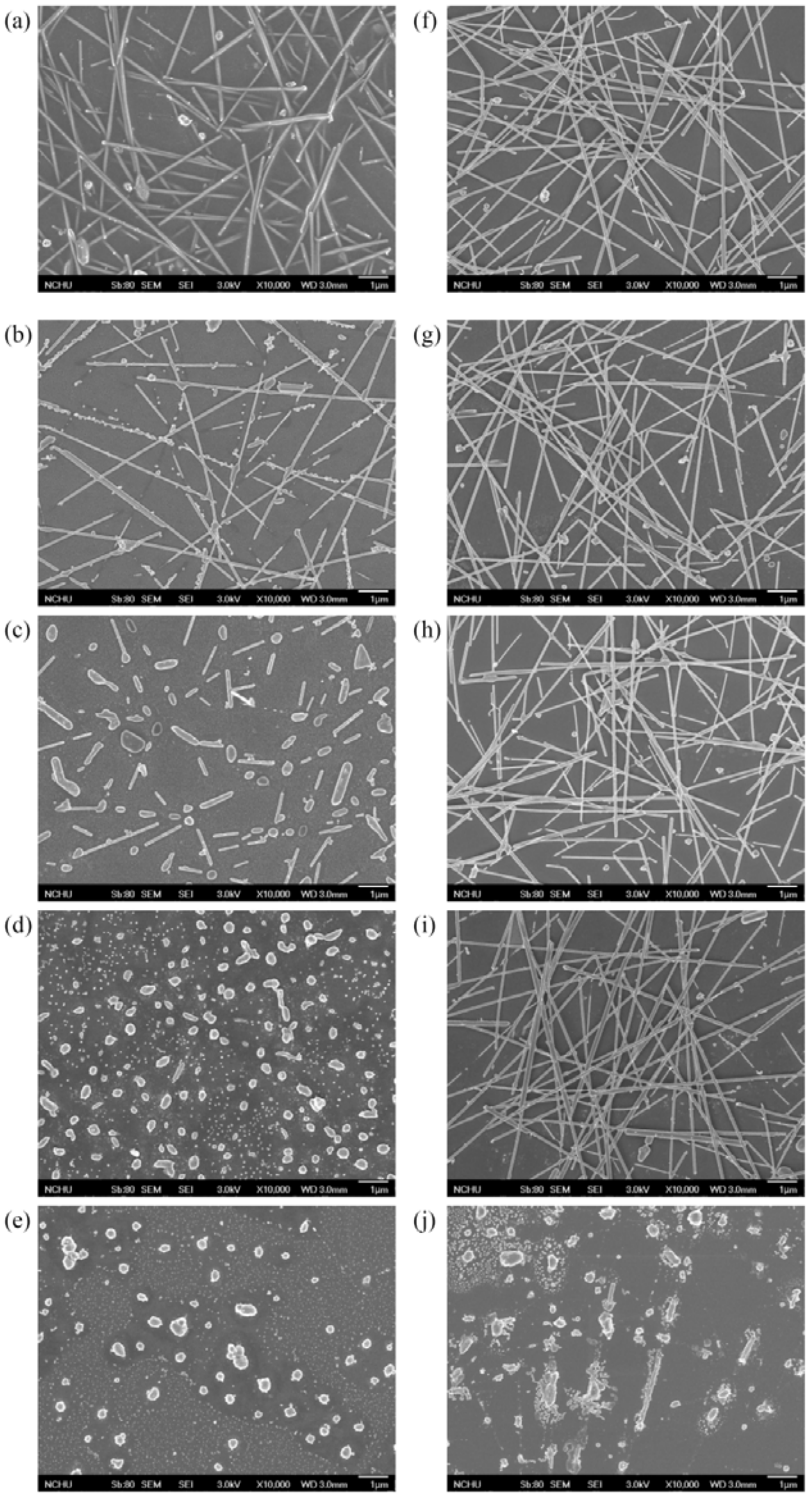

Fig. 3. SEM images of the AgNW electrodes treated thermally under (a-e) air and (f-j) N_2 atmospheres at various temperatures: (a, f) 200℃, (b, g) 250℃, (c, h) 300℃, (d, i) 400℃, and (e, j) 500℃.

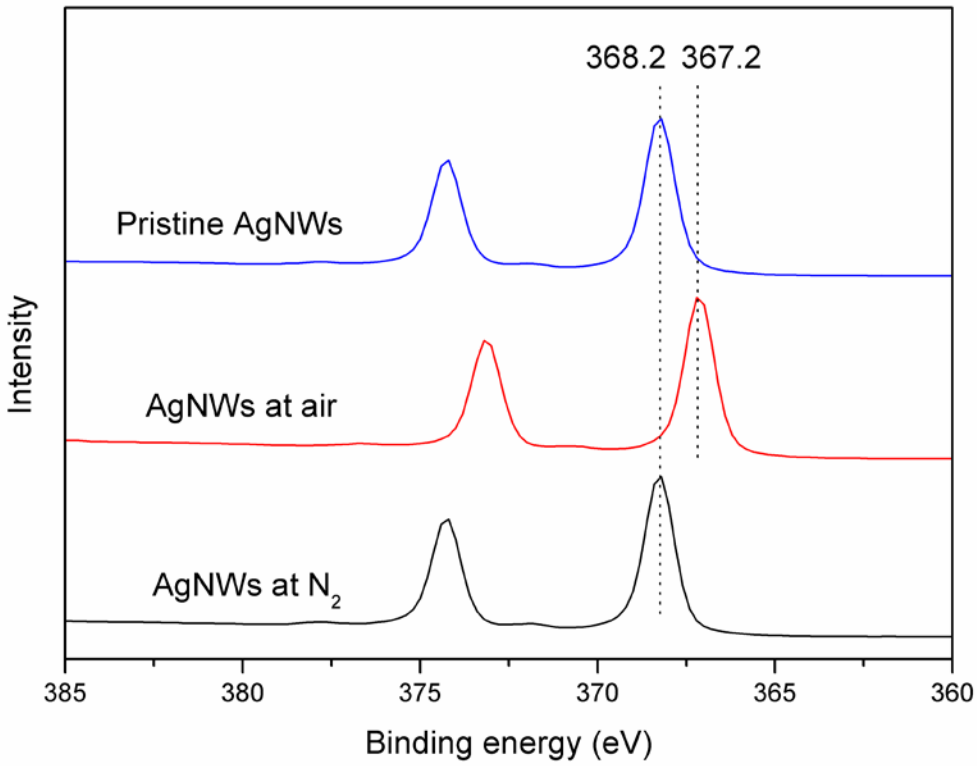

Fig. 4. XPS spectra of Ag_{3d} for the AgNW electrodes treated in various atmospheres.

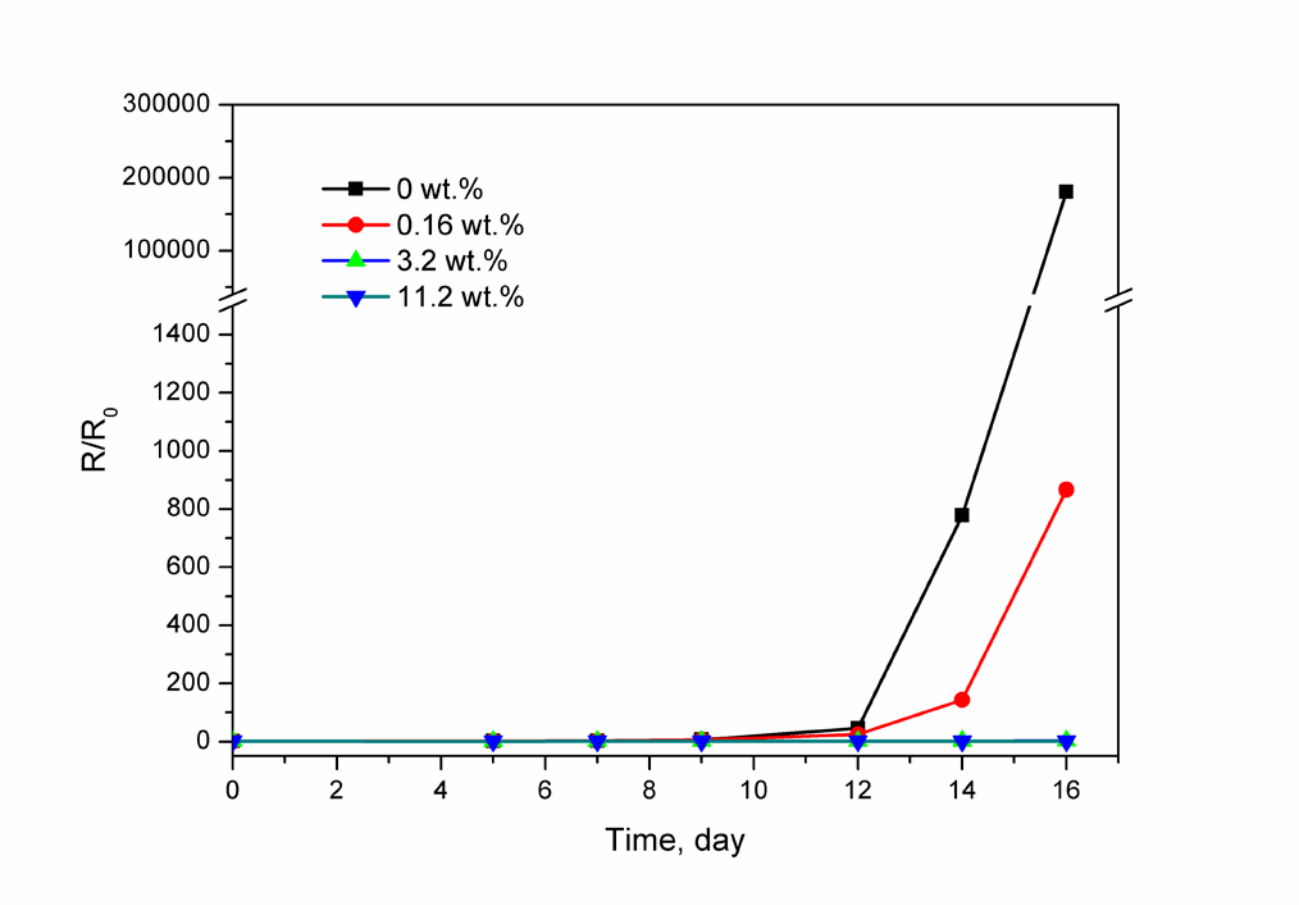

Fig. 5. Variation of the relative sheet resistance of the AgNW electrodes with various PES incorporation exposed to air at room temperature over time. R_0 is the initial sheet resistance, and R is the sheet resistance after exposure over time.

Fig. 6. Photographs of AgNW (left) and 3.2 wt.% PES-AgNW (right) electrodes exposed to air at room temperature over 15 days.

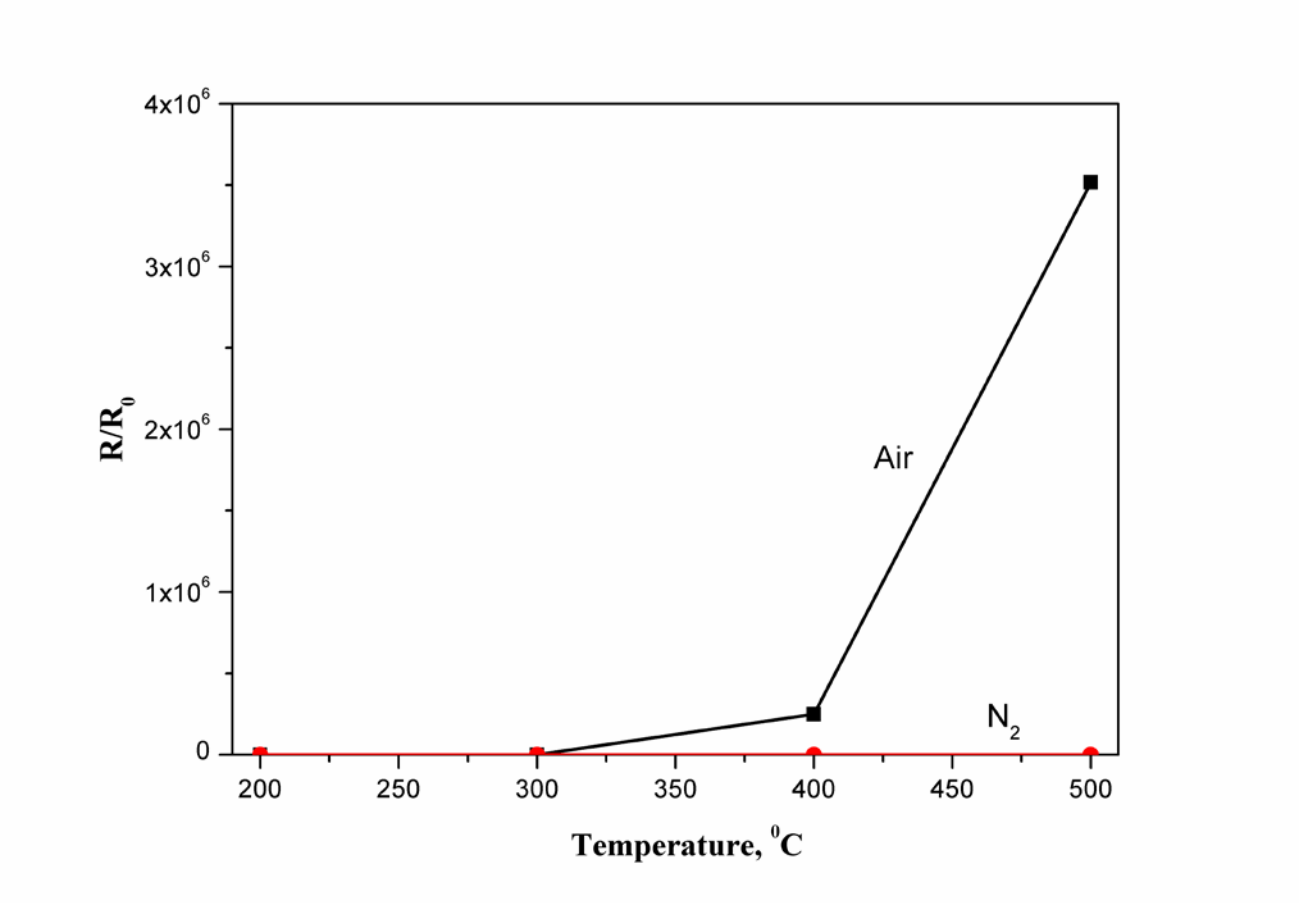

Fig. 7. Variation of the relative sheet resistance of the 3.2 wt.% PES-AgNW electrodes as a function of the thermal-treatment temperature under various atmospheres. R_0 is the initial sheet resistance, and R is the sheet resistance after thermal treatment.

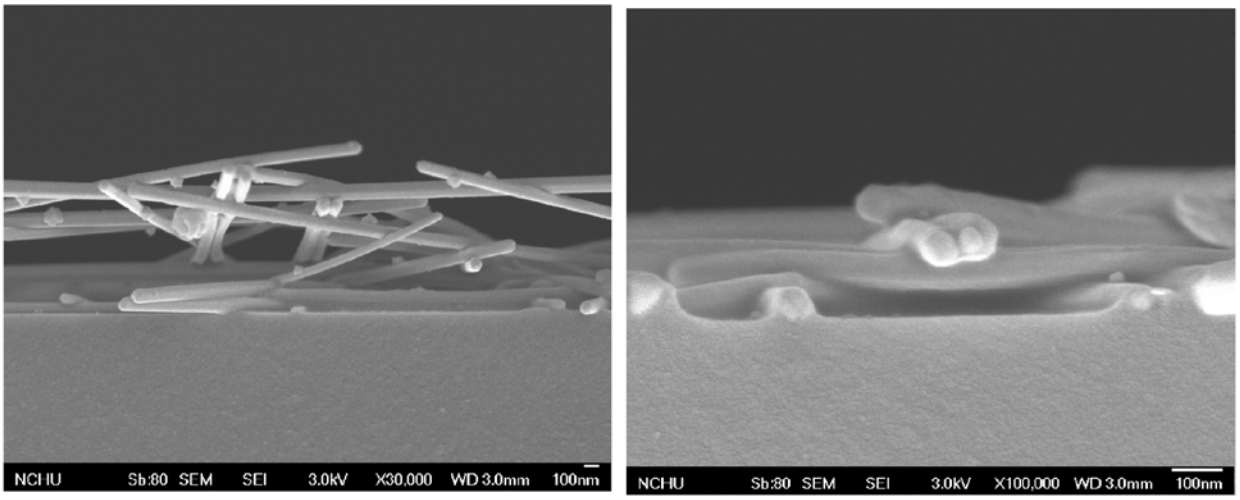

(a) (b)

Fig. 8. Cross-sectional SEM images of the AgNW electrodes (a) without and (b) with PES incorporation.

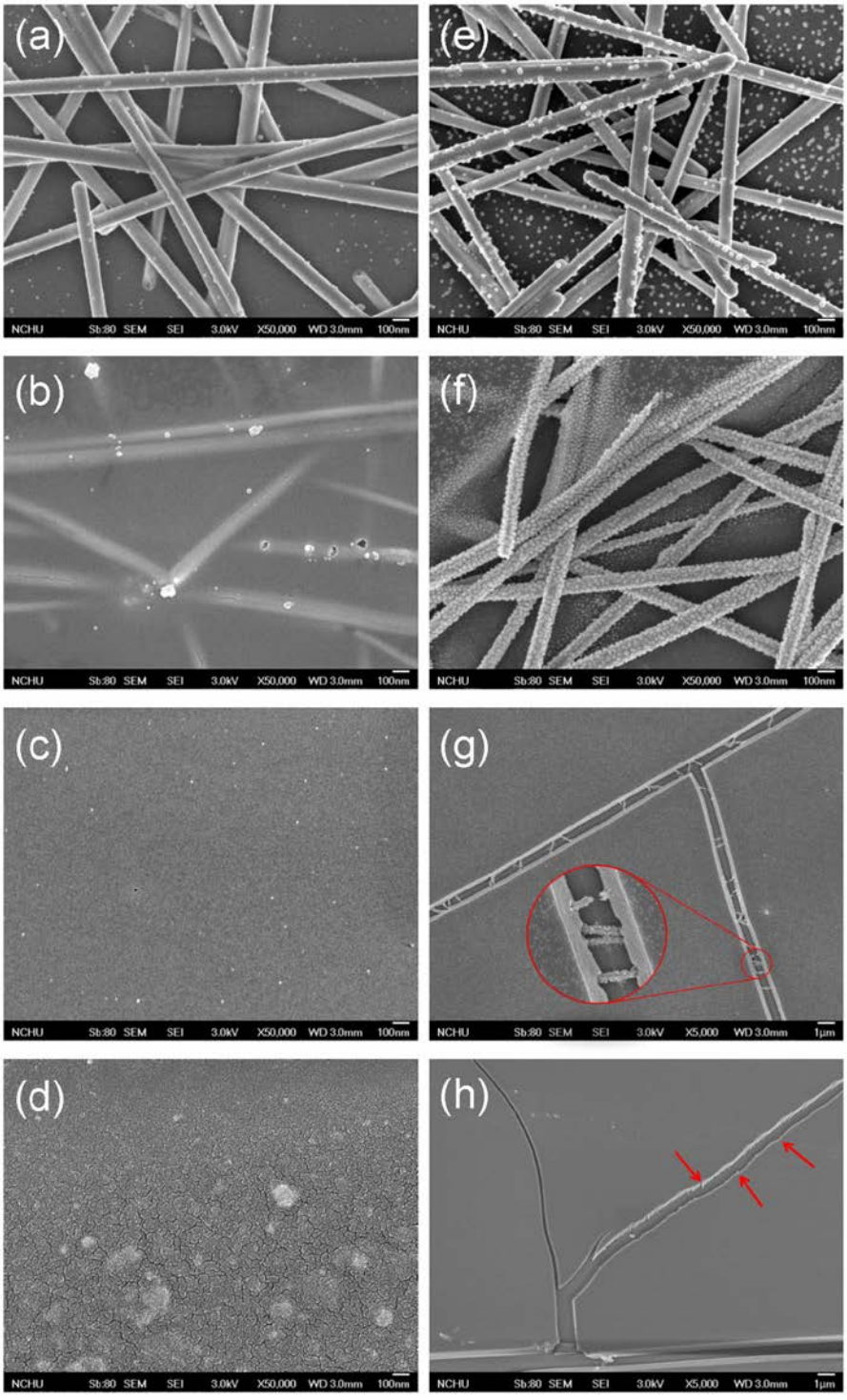

Fig. 9. SEM images of the AgNW electrodes dipped in various (a-d) PES and (e-h) TiO_2 concentrations: (a, e) 0.16 wt.%, (b, f) 1.6 wt.%, (c, g) 8 wt.%, and (d, h) 11.2 wt.%. The inset image in (g) and the arrows in (f) indicate the broken AgNWs.

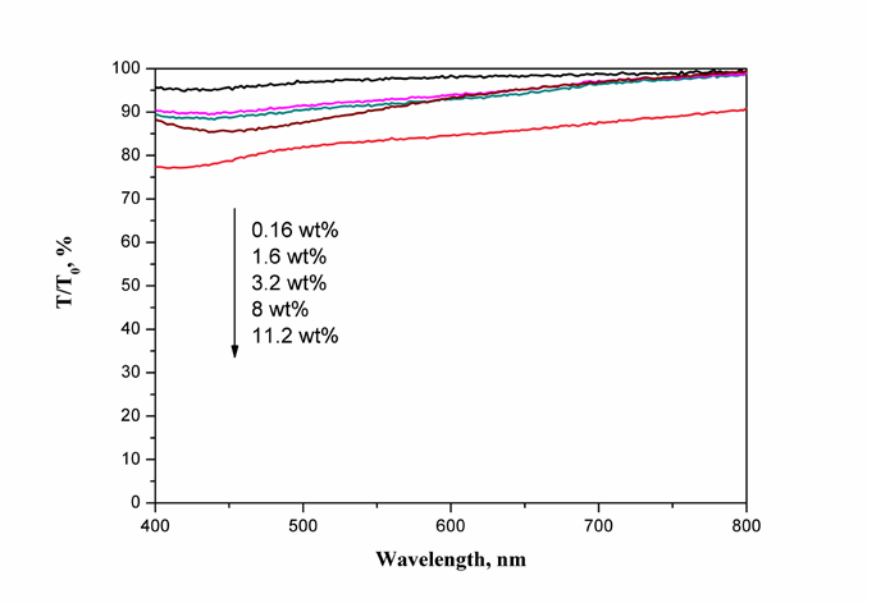

(a)

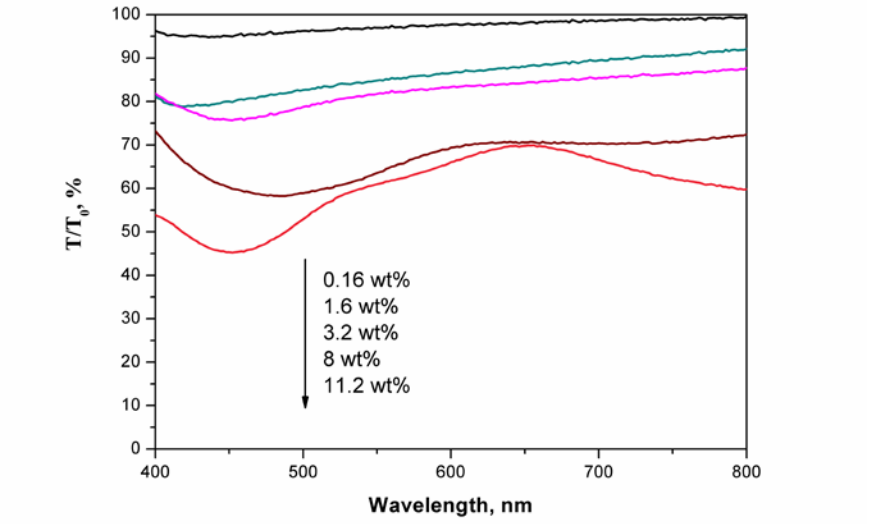

(b)

Fig. 10. Transmission spectra of the (a) PES-AgNW and (b) TiO_2-AgNW electrodes made from various dipping concentration.

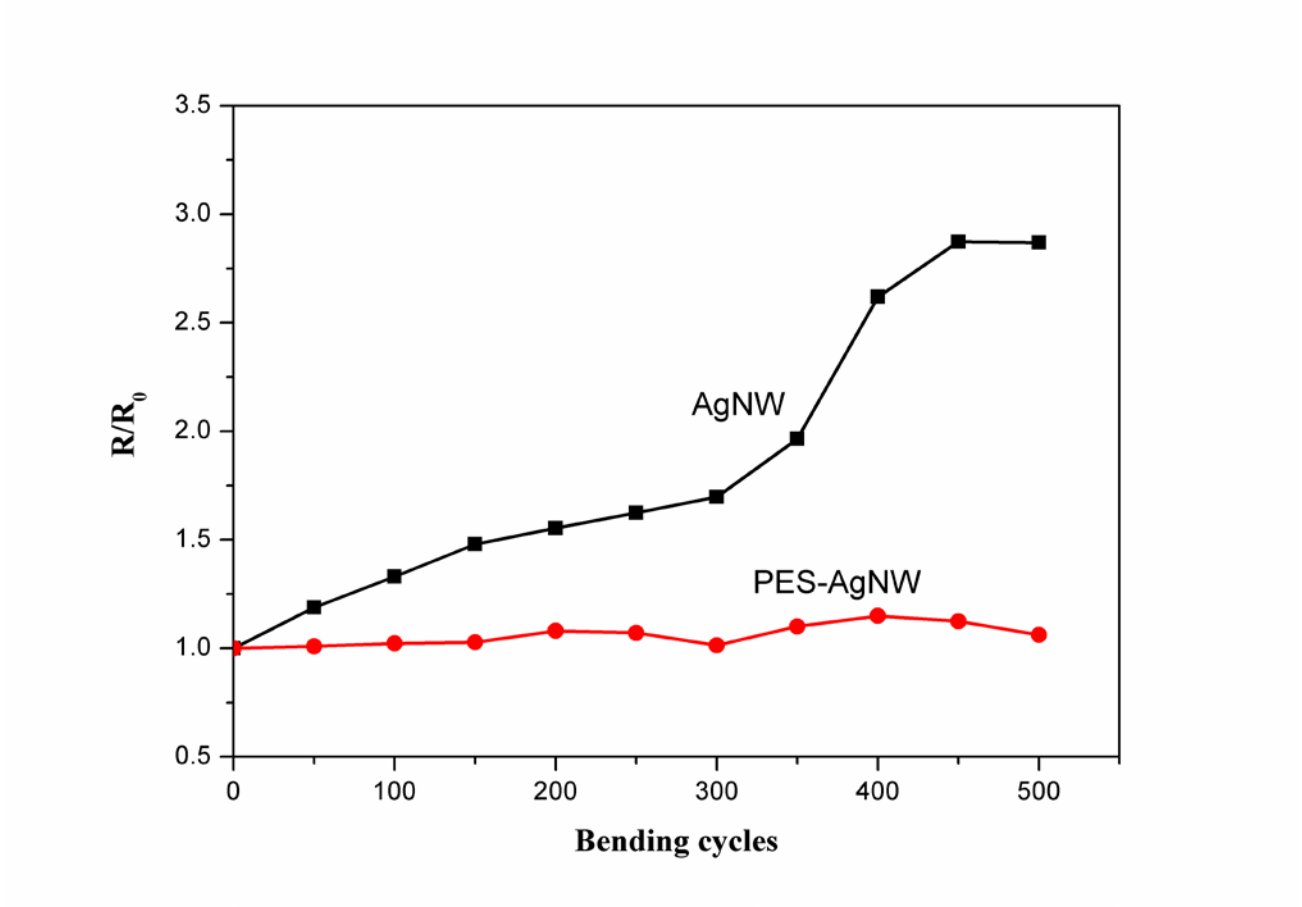

Fig. 11. Variation of the relative sheet resistance of the pristine AgNW electrode and the 3.2 wt.% PES-AgNW electrode as a function of bending cycles. R_0 is the initial sheet resistance, and R is the sheet resistance after the bending test.

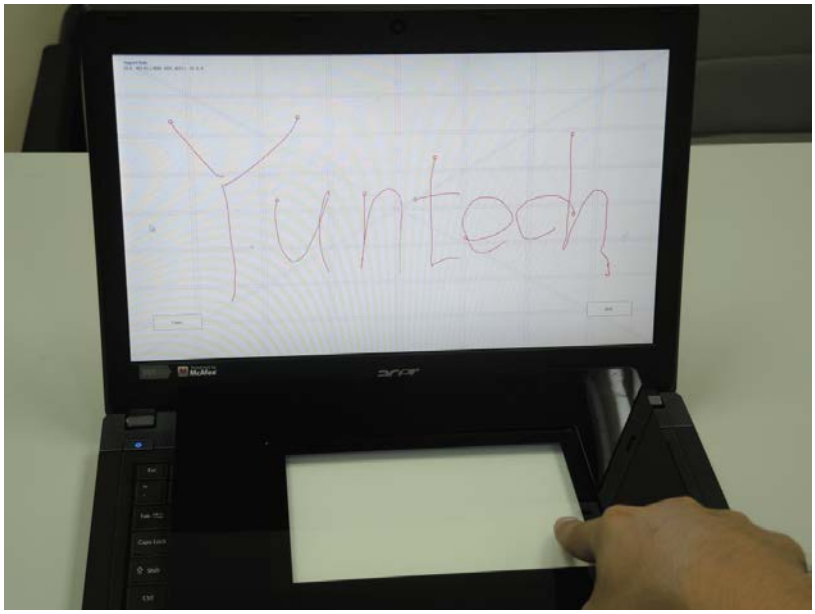

Fig. 12. Photograph of the touch sensor made from the PES-AgNW electrodes.